Nonlinear interferometers for broadband mid-infrared spectroscopy

Chiara Lindner, Sebastian Wolf, Jens Kießling, and Frank Kühnemann

Fraunhofer Institute for Physical Measurement Techniques IPM, Heidenhofstr. 8, 79110 Freiburg, Germany

ABSTRACT

Mid-infrared spectroscopy is one of the most important techniques in chemical analysis. However, the detectors for the mid-infrared range suffer from lower specific detectivities in comparison to their visible counterparts, cost more and often require cryogenic cooling. Nonlinear interferometers allow measuring mid-infrared spectra by detecting only visible light using the induced coherence effect. In our work, we realize a nonlinear interferometer designed for broadband mid-infrared spectra with high resolution, which is easily tunable, and in analogy to classical Fourier transform infrared (FTIR) spectrometers requires no additional spectral selection.

Keywords: Infrared spectroscopy, spontaneous parametric down-conversion, quantum optics, Fourier transform, nonlinear interferometer

1. INTRODUCTION

Nonlinear interferometers have recently sparked interest of a larger audience, as they offer the possiblity to measure information from less accessible spectral ranges with correlated visible light, for which high-performing and low-cost detectors are available. As a light source for correlated photons, typically spontaneous parametric down-conversion (SPDC) is used. This effect can be described as the spontaneous decay of a pump photon inside a nonlinear medium into two photons of lower energy, called signal and idler photon. Energy conservation requires that the sum of signal and idler frequency equals the pump photon frequency. All three waves have to be phase matched for an efficient conversion.

If two identical SPDC sources are pumped coherently and placed such that signal and idler photons are overlapped, interference in both signal and idler intensity is observable, as has been demonstrated by Zou et al. in 1991.[1] This might at first seem counter-intuitive, as SPDC is a spontaneous and incoherent process. The interference is due to the quantum-mechanical indistinguishability of the two photon pairs and has been called "induced coherence without induced emission". More interestingly, interference observed in the signal light disappears if the idler beams are made distinguishable. This effect is the basis of a new class of measurement arrangements, called nonlinear interferometers, wherein information on the state of the idler photons (transmission, phase, polarization change) is obtained by detecting the change in the signal interference pattern. This has been applied in quantum imaging,[2] optical coherence tomography[3,4] and polarimetry.[5]

Recently, the application of nonlinear interferometers for spectroscopy in the mid-infrared range has been demonstrated in several publications.[6–8] Different interferometric geometries were used: First, two nonlinear crystals placed in a row, resembling a classical Mach-Zehnder-interferometer.[6,7] In this geometry, the spectroscopic sample is passed by pump, signal and idler light and has to be transparent in pump and signal wavelength range. In a different geometry, the interferometer is formed by a single crystal, which is passed twice by all beams, resembling a Michelson-interferometer.[8] Hereby, the idler beam is separated from the pump and signal beams, which allows spectroscopy of materials independent of the transmission at pump and signal wavelengths.

The performance of a nonlinear interferometer as a spectroscopic measurement device is governed by the means of detecting the spectral information encoded in the signal interference patterns. So far, two methods have been demonstrated: The signal light can be analyzed with a spectrograph or spectrometer, for which resolutions of $20\,\mathrm{cm}^{-1}$ [Ref. 6] or $5.2\,\mathrm{cm}^{-1}$ [Ref. 8] have been demonstrated. Another method uses the known phase matching conditions in a numerical algorithm. Hereby, the resolution is limited to the bandwidth of the SPDC source, which in that case was as large as $80\,\mathrm{cm}^{-1}$ [Ref. 7].

in: Schunemann, P.G.; Schepler, K.L.; Society of Photo-Optical Instrumentation Engineers –SPIE: Nonlinear Frequency Generation and Conversion: Materials and Devices XIX. Proc. SPIE 11264, Paper 112641D (2020); doi: 10.1117/12.2545883

In our work, we demonstrate a different approach for obtaining the spectral information. In analogy to a classical Fourier-transform infrared spectrometer, the delay between the interferometer arms of our nonlinear Michelson-interferometer is varied. The spectral information is then obtained by a Fourier transform of the recorded interferograms. The spectral bandwidth of the SPDC source is increased by including non-collinear SPDC. The spectral resolution is only limited by the maximum optical path difference between the interferometer arms. This allows for measuring continuous spectra with a resolution of $6\,\mathrm{cm}^{-1}$ and a large spectral bandwidth of $100\,\mathrm{cm}^{-1}$ in a single measurement setting.

2. THEORY FRAMEWORK

SPDC can be described as the spontaneous decay of a pump photon with frequency ω_p and wave vector $\vec{k_p}$ into a correlated photon pair of a signal and idler photon with frequencies ω_s, ω_i and wave vectors $\vec{k_\mathrm{s}}$, $\vec{k_\mathrm{i}}$. The probability of generation is given by the modulus square of the biphoton field amplitude $F(\omega_\mathrm{s}, \vec{k_\mathrm{s}}, \omega_\mathrm{i}, \vec{k_\mathrm{i}})$. For a monochromatic, plane-wave pump inside a nonlinear crystal of length L, the signal photon amplitude is obtained by integrating over all idler modes, which results in:[9–11]

$$F^2(\omega_\mathrm{s}, \theta_\mathrm{s}) \propto \mathrm{sinc}^2\left(\frac{\Delta k L}{2}\right). \tag{1}$$

The phase mismatch Δk is described as a function of the signal frequency ω_s and the signal emission angle θ_s and can be calculated by its longitudinal (k_z) and vertical (k_x) components (for simplicity, the phase matching calculation is conducted in one representative plane of emission):

$$\begin{aligned} \Delta k_z &= k_\mathrm{p} - \frac{2\pi}{\Lambda} - k_\mathrm{s}\cos(\theta_\mathrm{s}) - k_\mathrm{i}\cos(\theta_\mathrm{i}) \\ \Delta k_x &= k_\mathrm{s}\sin(\theta_\mathrm{s}) - k_\mathrm{i}\sin(\theta_\mathrm{i}) \\ \Delta k &= \sqrt{\Delta k_x^2 + \Delta k_z^2} \end{aligned} \tag{2}$$

Hereby, $k_\mathrm{p,s,i} = 2\pi n_\mathrm{p,s,i}/\lambda_\mathrm{p,s,i}$ denote the lengths of the wave vectors for refractive indices $n_\mathrm{p,s,i}$ and wavelengths $\lambda_\mathrm{p,s,i}$ of pump, signal and idler light, respectively. For a nonlinear crystal with a poling period of Λ, the longitudinal phase mismatch component is reduced by $2\pi/\Lambda$. The idler emission angle θ_i is given by

$$\theta_\mathrm{i} = \arctan\left(\frac{k_\mathrm{s}\cdot\sin(\theta_\mathrm{s})}{k_\mathrm{p} - k_\Lambda - k_\mathrm{s}\cdot\cos(\theta_\mathrm{s})}\right). \tag{3}$$

Figure 1a) shows the signal photon amplitude as calculated by equation 1 for a pump wavelength of 532 nm and a 20 mm long lithium niobate crystal (poling period 10.6 µm, temperature 70 °C).

If the signal and idler beams of two coherently pumped SPDC sources are perfectly overlapped for interference in a scheme such as shown in Figure 2, the resulting signal photon amplitude can be described by[12]

$$|F(\omega_\mathrm{s}, \theta_\mathrm{s})|^2 \propto \mathrm{sinc}^2\left(\frac{\Delta k L}{2}\right)\left[1 + |\tau|\cdot\cos(\Delta\varphi)\right]. \tag{4}$$

As described before, the most interesting feature of a nonlinear interferometer is that the interference pattern of both signal and idler photons depends on the biphoton transmission (τ) and the phase difference between all three waves: $\Delta\varphi = \varphi_\mathrm{p} - \varphi_\mathrm{s} - \varphi_\mathrm{i}$. One contribution to the phase difference is the phase mismatch inside the nonlinear medium, given by $\Delta k \cdot L$. Additional phase difference is caused by different optical path lengths inside the nonlinear interferometer. Figure 1b) shows the signal photon amplitude for a nonlinear Michelson interferometer with a periodically poled lithium niobate crystal (same parameters as in Figure 1a), where the three perfectly collimated beams propagate for 90 mm and are reflected back into the nonlinear crystal. Hereby, the idler optical path is 1.4 mm longer than the pump and signal path.

The interference pattern is also visible in the projection of the signal photon amplitude to the angular axis, which can be measured with a spatially resolving, but spectrally nonselective detector. A polar plot of the projection of the signal amplitude from Figure 1b) is shown in Figure 1d). The projection of the calculated

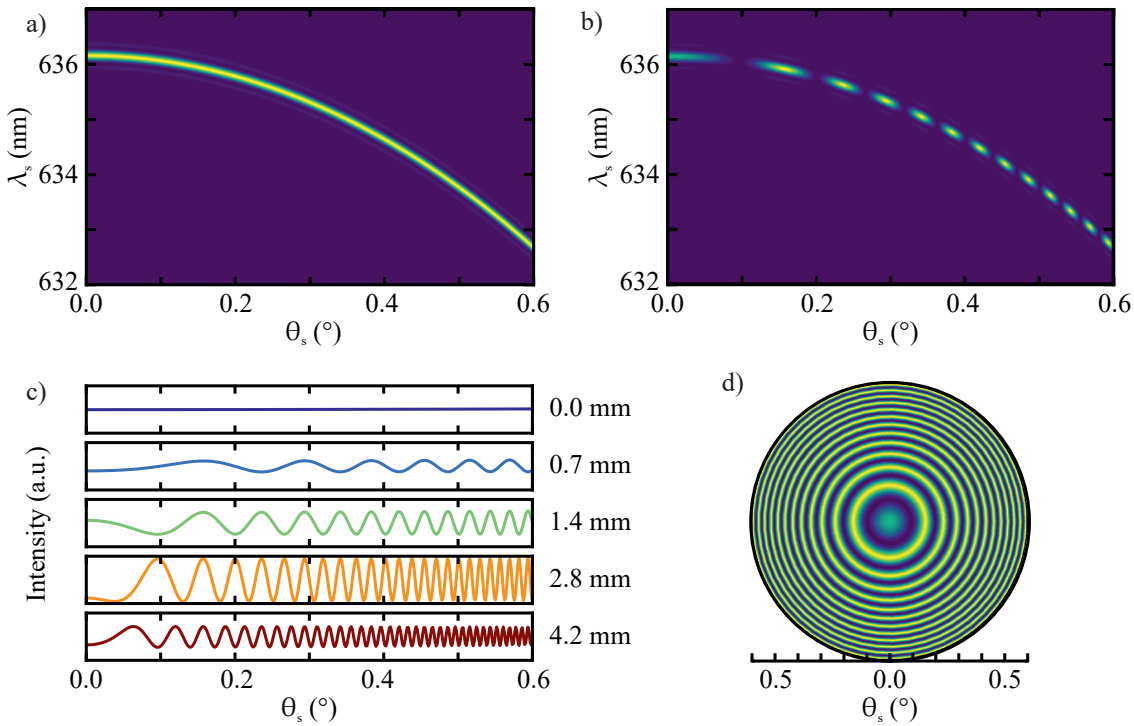

Figure 1. Calculated angular emission spectra of a nonlinear interferometer:
a) Spectrum of SPDC signal photons from a single source as function of the internal angle of noncollinear phase matching. Conditions: 20 mm long lithium niobate crystal with 532 nm pump wavelength, 10.6 µm poling period at 70 °C crystal temperature.
b) Interference pattern of two perfectly overlapped SPDC sources (same parameters as in a), as calculated by equation 4 for a path difference of 1.4 mm between idler and signal interferometer arm with a length of 180 mm.
c) Interference patterns projected to the emission angle axis for different idler path differences (denoted on the right).
d) Polar plot of the interference fringes corresponding to the two-dimensional pattern in b).

signal photon amplitude is shown in Figure 3c) as a function of the emission angle for different optical path differences (denoted on the right). The modulation reaches its highest contrast for an optical path difference of ca. 2.8 mm, which implies that the idler path has to be longer than the signal and pump interferometer arm to reach zero phase difference. This is caused by the dispersion of the nonlinear crystal. For longer optical path differences, the interference contrast decreases again, due to the limited coherence length of the SPDC emission. For the calculation, the interference contrast is equally high for all emission angles. It is to be noted, that this is only possible for perfect beam overlap, which was assumed for equation 4.

3. EXPERIMENTAL RESULTS

3.1 Set-up

A sketch of the nonlinear interferometer in Michelson configuration can be seen in Figure 2. As a pump source we use a laser with 532 nm wavelength, a linewidth of less than 1 MHz and 2 W output power (Coherent Verdi V2). The pumplaser passes an optical isolator and is focused to a beam waist of 120 µm at the center of the nonlinear crystal. The pump beam is reflected by a dichroic beamsplitter (DB_s) and passes through the nonlinear crystal. The nonlinear crystal is 20 mm long and consists of 5 % MgO-doped lithium niobate (PPLN). The crystal has 0.5 mm wide channels with different poling periods and is temperature stabilized using a peltier element.

Figure 2b) shows the phase matching curves (defined by $\Delta k = 0$) of three different poling periods and temperatures, which cover a signal wavelength range of 615 nm to 640 nm. The poling periods and temperatures

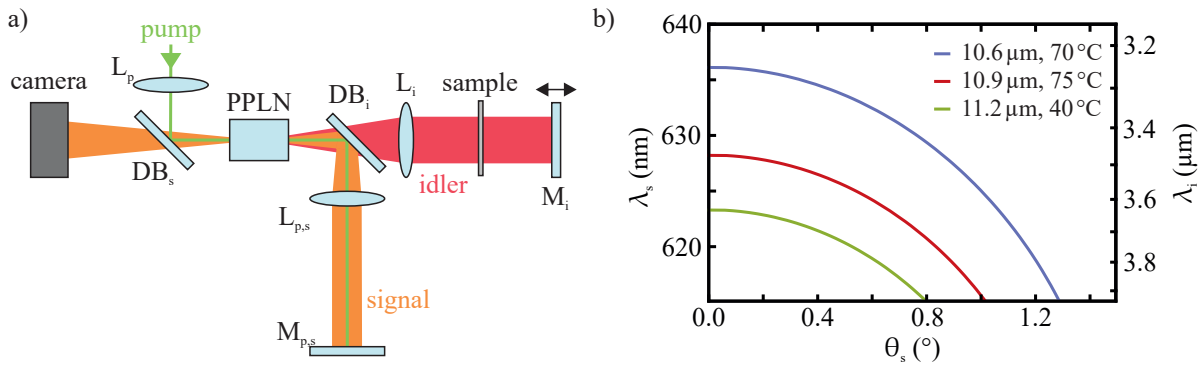

Figure 2. Experimental set-up:
a) Sketch of the nonlinear interferometer: "L" for lenses, "M" for plane mirrors, "DB" for dichroic beam splitters, the indices p,s,i indicate pump, signal and idler beam.
b) Phase matching curves (defined by $\Delta k = 0$) for three different poling periods and crystal temperature, with 532 nm pump wavelength.

correspond to the parameters used for a spectroscopic demonstration of the nonlinear interferometer with an idler wavelength range of 3.2 µm to 3.9 µm. The phase matching curves show that a large spectral bandwidth requires the imaging of a large signal emission angle range with sufficient mode overlap. In addition, it has to be considered, that the idler emission angles are larger than the signal emission angles ($\theta_\mathrm{i} = \lambda_\mathrm{i}/\lambda_\mathrm{s} \cdot \theta_\mathrm{s}$), and both angles are further increased due to refraction on the crystal surface.

Behind the nonlinear crystal, the three beams are separated with another dichroic beamsplitter ($\mathrm{DB_i}$). The idler light is transmitted and collimated with a 50 mm CaF_2 lens, then back reflected with a plane gold mirror placed in another 50 mm distance. The end mirror is mounted on a piezoelectric positioning system with 800 µm maximum displacement and a high position resolution of 1.8 nm. The positioning system moves the idler mirror in beam direction in order to vary the optical path length. A spectroscopic sample can be placed inside the collimated part of the idler beam. The pump and signal light are reflected by the dichroic beam splitter and take an analogue path with a fixed length. All three beams re-enter the nonlinear crystal, and interference becomes observable in the signal and idler light, if the spatial modes are sufficiently overlapping. Behind the nonlinear crystal, the pump is reflected at the dichroic beam splitter ($\mathrm{DB_s}$) and removed by the isolator. The signal beam is transmitted by the beam splitter, and passes several spectral filters removing pump, idler and ambient light. The signal interference pattern is then measured without any spectral selection with a silicon sCMOS camera (Andor Zyla 4.2, with a resolution of 2048x2048 pixels).

3.2 Measurement and analysis

Figure 3a) shows the interference pattern of a measurement taken with a poling period of 10.6 µm and a crystal temperature of 70 °C, which corresponds to the parameters of the blue phase matching curve in Figure 2b). The interference pattern is visible in ring segments. We attribute the missing parts of the interference patterns to the narrow aperture of the crystal in vertical direction. The colored dots mark positions on the camera sensor which correspond to the internal signal emission angles denoted on the right. The emission angles were calculated by $n \cdot \tan(\theta_\mathrm{s}) = R/D$, with the radial distance R to the center of the interference pattern, the distance D =80 mm between the nonlinear crystal and the camera sensor and a refractive index of $n \approx 2.2$.

For a measurement of the idler spectral density, the optical path length of the idler interferometer arm is varied by the piezo positioning system, which moves the idler mirror. Each step of displacement, a camera image such as the one shown in Figure 3a) is recorded. The positioning system allows a maximum displacement of 800 µm, which corresponds to an optical path difference of 1.6 mm. Figure 3b) shows the intensity trace along the idler mirror displacement for the five different positions on the camera (marked in the corresponding color in figure 3a). The curves are shifted for clarity. At the center of the interference pattern, the modulation remains visible along the whole displacement range. For collinear emission, an interference contrast of over 50 %

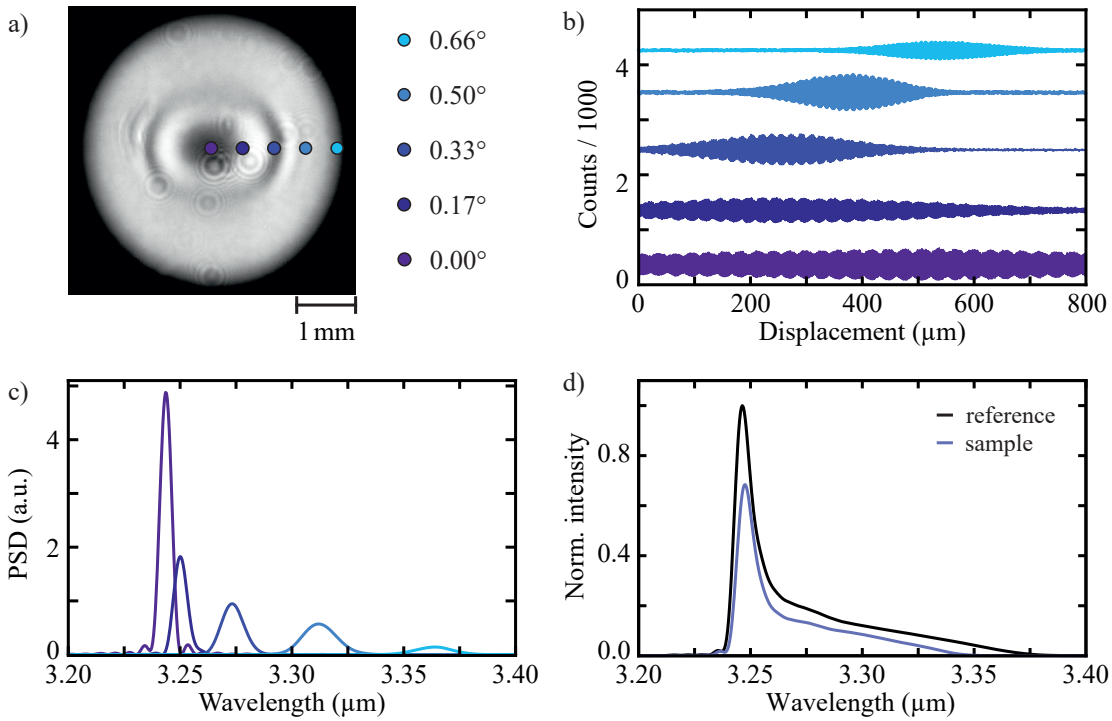

Figure 3. Measurement and analysis of the signal interference patterns:
a) Interference pattern measured with 10.6 µm poling period at 70 °C crystal temperature. Marked with colored dots are five positions on the camera, which correspond to the internal signal emission angles denoted on the right.
b) Measured intensity at the positions marked with dots of the same color in a). The interferograms are shifted for clarity.
c) Fourier-transformed spectra (power spectral density) of the interferograms shown in b)
d) Idler spectrum of the nonlinear interferometer, calculated by the sum over the partial spectra of all camera pixels, without (black line) and with (blue) a measurement sample introduced into the idler interferometer arm.

is achieved. With increasing distance to the center, the envelope of the interferograms becomes narrow and the point with highest interference contrast shifts to larger displacement values.

The interferograms can be compared to the interference patterns and their projections as shown in figure 1, which were calculated for the parameters of the experiment (crystal material and length, poling period, temperature, propagation length, pump wavelength). The calculated interference pattern (Fig. 1d) resembles the measured pattern for the central region to some degree. However, in comparison, the measured interference pattern shows a fast decreasing interference contrast for non-collinear emission. The fine ring structure, which is visible in the calculation, is not resolved in the measured pattern. This might be caused by imaging errors, which affect non-collinear emission stronger and decrease the mode overlap of both signal and idler beams. For the non-collinear interferograms shown in figure 3b), interference contrast is only visible within a narrow window, while the calculated projected patterns from Figure 1c) show a constantly high contrast over the whole emission angle range. The partial decrease of visibility observed in the experiment could be caused by the length of the crystal, which prevents a perfect collimation of the SPDC emission. A slightly divergent beam is imaged onto the camera with varying optical path differences for the different divergence angles, which decreases the interference contrast. This is related to the self-apodization effect known for classical Fourier-transform infrared spectrometry.[13]

Figure 3c) demonstrates how the spectral information is extracted from the interferograms. Hereby, the partial spectrum of the interferogram of each camera pixel is calculated by a discrete Fourier transform. The Fourier transformed spectra of the interferograms from Figure 3b) are shown in Figure 3c) in the same color.

Moving from the center the Fourier transformed spectra are shifted towards larger wavelengths, which is in agreement to the phase matching curve, as shown in figure 2b). For the collinear interferogram, sidebands are visible, which are caused by the limited displacement range, which acts like a rectangular window function. From these five spectra, we can estimate the spectral range that is covered in a single measurement setting to over $100\,\mathrm{cm}^{-1}$.

The complete idler spectrum of the interferometer is calculated by the sum over the Fourier transformed spectra of all camera pixels. The black line in Figure 3d) shows the reference idler spectrum, which was measured without a spectroscopic sample inside the idler interferometer arm. The spectrum shows maximum intensity at the collinear wavelength at 3.25 µm. The intensity decreases rapidly for larger wavelengths, which is caused by the decreasing interference contrast for larger emission angles. For measuring the transmission of a spectroscopic sample, the measurement procedure is repeated with the sample placed into the collimated idler beam. For demonstration we chose a polypropylene film with a strong absorption band around 3.4 µm. The spectrum measured with the sample is shown in Figure 3d) as the blue curve. The transmission T is calculated from the reference I_r and sample I_s spectrum by

$$T = \sqrt{\frac{I_\mathrm{s}}{I_\mathrm{r}}} \tag{5}$$

since the sample is passed twice inside the interferometer. Both reference and sample spectrum are restricted to the non-collinear spectral range where no sidebands of the Fourier transformed spectra occur. Additionally, the transmission is only calculated where the reference spectrum surpasses a threshold of 2 % of its maximum value. The measurements were repeated for the other two phase matching configurations shown in Figure 2b (red and green curve). For comparison with a conventional method of MIR spectroscopy, the transmission of the polypropylene sample is also measured with a Fourier-transform infrared spectrometer (Bruker Vertex 80, 64 scans at a resolution of $0.5\,\mathrm{cm}^{-1}$).

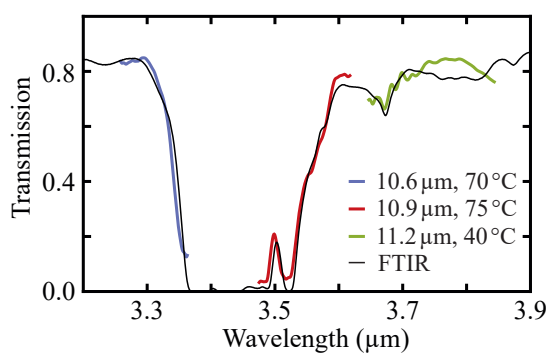

Figure 4. Transmission spectrum of a thin polypropylene film. Black line: Measurement taken with a commercial Fourier-transform infrared spectrometer. Colored lines: Transmission calculated from the spectra measured with the nonlinear interferometer, using different phase matching conditions denoted by the poling period and crystal temperature.

The experimental results are shown in figure 4. The spectrum measured with the commercial Fourier transform infrared spectrometer is shown in black. The colored lines show the transmission measured with the nonlinear interferometer for three different poling periods and crystal temperatures, as calculated by equation 5. The spectra show good agreement with the reference FTIR measurement. Each segment of the spectrum covers a bandwidth of more than $100\,\mathrm{cm}^{-1}$. The spectral resolution is theoretically limited to $6\,\mathrm{cm}^{-1}$, due to the maximum idler mirror displacement of 800 µm and can be increased by using a larger mirror displacement range. The spectral resolution is comparable to the resolution demonstrated in Ref. 8.

4. CONCLUSION

We demonstrated MIR spectroscopy enabled by the combination of a nonlinear interferometer with a Fourier transform approach extracting the spectral information. While the mid-infrared idler photons interact with the sample, the interferograms are recorded by detecting the correlated visible signal photons. This allows the use

of silicon-based detectors rather than expensive and often cryogenically cooled detectors. In contrast to other measurement techniques using nonlinear interferometers for MIR-spectroscopy, our set-up requires no spectrally selective detection or beforehand knowledge on the phase matching properties of the crystal. The current resolution is comparable to the state of the art ($5.2\,\mathrm{cm}^{-1}$)[7] and can be improved by increasing the maximum path differences of the interferometer. The technique can be easily extended to the whole infrared transparency range of lithium niobate. Possibly it could be extended to the FIR and terahertz range.[14] We believe that the presented approach, the combination of a nonlinear interferometer and Fourier-analysis will provide a more accessible way of MIR-spectroscopy with visible photons.

REFERENCES

[1] Zou, X. Y., Wang, L. J., and Mandel, L., "Induced coherence and indistinguishability in optical interference," *Physical review letters* **67**(3), 318–321 (1991).

[2] Lemos, G. B., Borish, V., Cole, G. D., Ramelow, S., Lapkiewicz, R., and Zeilinger, A., "Quantum imaging with undetected photons," *Nature* **512**(7515), 409–412 (2014).

[3] Vanselow, A., Kaufmann, P., Zorin, I., Heise, B., Chrzanowski, H., and Ramelow, S., "Mid-infrared frequency-domain optical coherence tomography with undetected photons," *Quantum Information and Measurement (QIM) V: Quantum Technologies* , T5A.86, Optical Society of America (2019).

[4] Paterova, A. V., Yang, H., An, C., Kalashnikov, D. A., and Krivitsky, L. A., "Tunable optical coherence tomography in the infrared range using visible photons," *Quantum Science and Technology* **3**(2), 025008 (2018).

[5] Paterova, A., Yang, H., An, C., Kalashnikov, D., and Krivitsky, L., "Polarization effects in nonlinear interference of down-converted photons," *Optics express* **27**(3), 2589–2603 (2019).

[6] Kalashnikov, D. A., Paterova, A. V., Kulik, S. P., and Krivitsky, L. A., "Infrared spectroscopy with visible light," *Nature Photonics* **10**(2), 98–101 (2016).

[7] Paterova, A., Lung, S., Kalashnikov, D. A., and Krivitsky, L. A., "Nonlinear infrared spectroscopy free from spectral selection," *Scientific reports* **7**, 42608 (2017).

[8] Paterova, A., Yang, H., An, C., Kalashnikov, D., and Krivitsky, L., "Measurement of infrared optical constants with visible photons," *New Journal of Physics* **20**(4), 043015 (2018).

[9] Byer, R. L. and Harris, S. E., "Power and bandwidth of spontaneous parametric emission," **168**(3), 1064–1068 (1968).

[10] Kleinman, D. A., "Theory of optical parametric noise," *Physical Review* **174**(3), 1027–1041 (1968).

[11] Klyshko, D., [*Photons Nonlinear Optics*], Taylor & Francis (1988).

[12] Chekhova, M. V. and Ou, Z. Y., "Nonlinear interferometers in quantum optics," *Advances in Optics and Photonics* **8**(1), 104 (2016).

[13] Griffiths, P. R. and de Haseth, J. A., [*Fourier transform infrared spectrometry*], Wiley-Interscience (2007).

[14] Kutas, M., Haase, B., Bickert, P., Riexinger, F., Molter, D., and von Freymann, G., "Terahertz quantum sensing," *arXiv:1909.06855* (2019).